Direct ab Initio Dynamics Studies of the Hydrogen Abstraction Reactions of Hydrogen Atom with Fluoromethanes

Dilip K. Maity, Wendell T. Duncan, and Thanh N. Truong*

Henry Eyring Center for Theoretical Chemistry, Department of Chemistry, University of Utah, Salt Lake City, Utah 84112

Received: October 30, 1998; In Final Form: January 19, 1999

A direct ab initio dynamics study on the gas-phase reactions of atomic hydrogen with different fluoromethanes has been carried out. The thermal rate constants were calculated using canonical variational transition state (CVT) theory augmented by multidimensional semiclassical zero and small curvature tunneling approximations. The potential energy surfaces for the reactions were calculated using hybrid density functional theory, namely, Becke's half-and-half (BH) nonlocal exchange and the Lee−Yang−Parr (LYP) nonlocal correlation functionals using the cc-pVDZ basis set. The reaction energies and barrier heights were improved by single-point energy calculations along the minimum energy path (MEP) at the spin-projected fourth order Moller−Plesset perturbation theory (PMP4) using the cc-pVTZ basis set. The calculated forward and reverse thermal rate constants are in the good agreement with the experimental data. The electronic effects of fluorine substitution on the rate of this class of reactions are examined.

Introduction

Halons (chlorofluorobromocarbons) have been widely used as a chemical fire extinguisher in ships, aircraft, and computer rooms; however, their production and use are banned worldwide because of their destructive effects on stratospheric ozone. It is understood that the ozone depletion potential of halons is caused by bromine. As an alternative to halons, hydrofluorocarbons (HFC) have been proposed as fire suppressants. These compounds contain no chlorine or bromine, and fluorine is believed to be relatively innocuous in its effect on the ozone layer.[1,2] Among the hydrocarbons, fluorinated methanes are considered to be safe alternative potential candidates as flame suppressants.[3,4] Accurate kinetic data for the reactions of hydrogen atoms with fluorinated methanes are needed to assess the mechanism and effectiveness for their use as alternative flame suppressants and to model the combustion chemistry of fluorinated hydrocarbons. The reliability of computational kinetic modeling is critically dependent on the accuracy of estimated rate constants for the different channels of the reactions involving these species under combustion temperatures. Unfortunately, the required kinetic data are often unavailable or else have been obtained at only a few temperatures.

Recent work has indicated that the abstraction of hydrogen atoms from fluoromethanes by H atoms is one of the major destruction pathways in a flame, and therefore, a basic understanding of this process may help in designing more effective fire suppression agents. Three different pathways for the reaction of H atoms with CH_3F, CH_2F_2, and CHF_3 have been discussed in the literature because of their exothermicities: abstraction of H ($CH_{4-x}F_x + H \leftrightarrow CH_{3-x}F_x + H_2$), abstraction of F ($CH_{4-x}F_x + H \leftrightarrow CH_{4-x}F_{x-1} + HF$), and substitution ($CH_{4-x}F_x + H \leftrightarrow CH_{5-x}F_{x-1} + F$). It has also been shown in the literature, based on ab initio molecular electronic structure calculations at various levels of theory, that the reactions of F abstraction or substitution have much higher barriers compared to the H abstraction reaction channel, thus making those two channels minor.[5] For this reason, in our present study, we focus only on the H abstraction reaction channel ($CH_{4-x}F_x + H \leftrightarrow CH_{3-x}F_x + H_2$; $x = 1$, 2, or 3), at a fairly accurate level of calculation. To examine the electronic effect of fluorine substitution and for the sake of comparison, we have also presented results for the H abstraction reaction of methane ($x = 0$) at the same level of theory.

To date, unlike the $H + CH_4$ reaction, only a limited number of experimental measurements of the thermal rate constants are available for H abstraction reactions of fluoromethanes. However, for purpose of comparison in this study we use several sets of experimental data available in the literature at different temperatures for these four reactions.[6−19] Several previous groups[20−22] have looked at the equilibrium structures, but only Berry et al.[5] have studied the kinetics of the $H + CH_{4-x}F_x$ ($x = 0-3$) reactions using conventional transition state theory (TST). Recently, Hranisavljevic and Michael[19] have also studied the reaction $CHF_3 + H \leftrightarrow CF_3 + H_2$, theoretically also employing TST with one-dimensional Eckart tunneling corrections. It is known that tunneling contributions in hydrogen abstraction reactions are significant. Thus, one-dimensional tunneling models associated with the TST framework may not be sufficient. Variational transition state theory[23] provides a framework for more accurate tunneling treatments. Since an analytical potential energy function for these reactions is not available, the conventional approach of reactive dynamic calculations is not viable.[23] Direct dynamics approach provides a viable alternative for using the more extensive variational transition state theory and tunneling methods to obtain accurate thermal rate constants.[24,25] In this approach, all potential information required for evaluating dynamic properties are obtained directly from ab initio electronic structure calculations rather than from empirical analytical force fields.

In the present study, we employ the direct ab initio dynamics[26−30] method developed in our laboratory to obtain thermal rate constants for H abstraction reactions and look into the substitution effects of fluorine on the rate of H atom transfer reaction.

10.1021/jp984281x CCC: $18.00
Published on Web 03/13/1999

Theory

I. Variational Transition State Theory. The variational transition state rate constants for a gas-phase bimolecular reaction is determined by varying the location of the dividing surface along a reference path to minimize the rate, thus keeping a possibility to minimize the error due to "recrossing" trajectories.[31,32] In the present study, the reference path is the minimum energy path (MEP) which is defined as the steepest descent path from the saddle point to both the reactant and product sides in the mass weighted Cartesian coordinate system. The reaction coordinate, s is defined as the distance along the MEP with the origin located at the saddle point and is positive on the product side and negative on the reactant side. For canonical ensemble at a given temperature T, the canonical variational theory (CVT) thermal rate constant is given by

$$k^{\mathrm{CVT}}(T,S) = \min_{s}\{k^{\mathrm{GT}}(T,S)\} \tag{1}$$

where

$$k^{\mathrm{GT}}(T,s) = \left\{\sigma\frac{k_{\mathrm{B}}T}{h}\frac{Q^{\mathrm{GT}}(T,S)}{\Phi^{\mathrm{R}}(T)}\mathrm{e}^{-V_{\mathrm{MEP}}(s)/k_{\mathrm{B}}T}\right\} \tag{2}$$

In these equations, $k^{\mathrm{GT}}(T,s)$ is the generalized transition state theory rate constant at the dividing surface which intersects the MEP at s and is orthogonal to the MEP at the intersection point. Q^{GT} is the internal partition function of the generalized transition state with the local zero of energy at $V_{\mathrm{MEP}}(s)$, which is the classical potential energy along the minimum energy path s with its zero of energy at the reactants. Φ^{R} is the reactant partition function per unit volume for bimolecular reactions. σ is the symmetry factor accounting for the possibility of more than one symmetry related reaction path and can be calculated as the ratio of the product of the reactant rotational symmetry numbers to that of the transition state. k_{B} is Boltzman's constant and h is Plank's constant. Both the Q^{GT} and Φ^{R} are approximated as products of electronic, rotational, and vibrational partition functions. For Φ^{R}, the relative translational partition function is also included. Translational and rotational partition functions were evaluated classically, whereas, the vibrational partition functions were calculated quantum mechanically within the harmonic approximation for the present studies. To include the quantal effects for motion along the reaction coordinate, CVT rate constants are multiplied by a transmission coefficient, $\kappa(T)$; thus, the final rate constant is given by

$$k(T) = \kappa(T)k^{\mathrm{CVT}}(T) \tag{3}$$

II. Multidimensional Semiclassical Tunneling Methods. The effective potential for tunneling is approximated as the vibrationally adiabatic ground-state potential, which has the form

$$V_{\mathrm{a}}^{G}(s) = V_{\mathrm{MEP}}(s) + \sum_{i=1}^{3N-7}\frac{1}{2}h\omega_i(s) \tag{4}$$

The transmission coefficients are calculated with multidimensional semiclassical zero and small curvature tunneling methods,[25,32−35] denoted as ZCT and SCT, respectively. The SCT transmission coefficients, which include the reaction path curvature effect on the transmission probability, are based on the centrifugal-dominant small-curvature semiclassical adiabatic ground-state approximation. In particular, the transmission probability at energy E, $P(E)$ is given by

$$P(E) = \frac{1}{\{1 + \mathrm{e}^{2\theta(E)}\}} \tag{5}$$

where $\theta(E)$ is the imaginary action integral evaluated along the tunneling path,

$$\theta(E) = \frac{2\pi}{h}\int_{s_1}^{s_r}\sqrt{2\mu_{\mathrm{eff}}(s)|E - V_a(s)|}ds \tag{6}$$

and where the integration limits, s_{l} and s_{r}, are the reaction coordinate turning points. The reaction-path curvature effect on the tunneling probability is included in the effective reduced mass μ_{eff}. Thus, the ZCT transmission coefficients are obtained by setting μ_{eff} equal to μ in the above equation. The detailed descriptions on the VTST and tunneling methods are presented elsewhere.[31−34]

Computational Details

It has been shown earlier that the combination of Becke's half-and-half (BH) with Lee−Yang−Parr (LYP) correlation functionals can be used cost effectively to calculate the geometries and Hessians along the MEP particularly for open-shell systems.[26,30,36] In our present study, we have adopted BHLYP method as implemented in the GAUSSIAN program[37] to determine structure and Hessian information using the cc-pVDZ basis set. To investigate the effects of the basis set on the calculated geometry, the cc-pVTZ basis set was also employed. It has been observed that the DFT energies are not always sufficiently accurate for rate calculations. To obtain more accurate information on energy, spin-projected fourth-order Moller−Plesset perturbation theory (PMP4) calculations are performed using a larger cc-pVTZ basis set. The minimum energy path (MEP) calculations are done in the mass weighted Cartesian coordinate with the sufficiently small step size of 0.01 amu$^{1/2}$ bohr for a total of 200 steps using the Gonzalez−Schlegel method.[38] This step size is found to be sufficient for the convergence of the variational rate constant as mentioned in our previous study.[25] For rate calculations, 21 Hessian grid points along the MEP were selected using the automated focusing technique. This technique uses a combination of the barrier shape, and the second derivatives of the Z-matrix geometrical parameters to predict the regions along the MEP that are sensitive in rate determination.[25] To improve the energetic information along MEP, single-point PMP4/cc-pVTZ calculations at six different selected points along MEP were performed. These points were generated by an automated method as implemented in our program, TheRate.[25] The PMP4 potential energy curve along the entire MEP is calculated by adding the corrections to the DFT potential energy curve. The location of the maximum on this improved potential energy curve is shifted slightly from the saddle point calculated from the BHLYP method. Thus for rate calculations, the origin of the reaction coordinate s is readjusted to zero in the present variational transition state rate calculations, so that the proper variational effects are reflected.

Results and Discussion

I. Stationary Points. Table 1 lists the computed and experimental geometrical parameters of the species at their equilibrium positions. For most species, the geometrical parameters calculated at cc-pVDZ basis set are found to be reasonably close to those calculated at the larger cc-pVTZ basis set. Furthermore, except for H_2, BHLYP/cc-pVDZ results agree better with the available experimental data. In particular, for

TABLE 1: Calculated and Experimental Geometrical Parameters (Distances in angstroms and Angles in degrees) of Stable Structures

	geometrical parameters	BHLYP/ cc-pVDZ	BHLYP/ cc-pVTZ	exptl
H−H	r_{HH}	0.754	0.737	0.741
CH_3	r_{CH}	1.083	1.071	1.079
(D_{3h})	∠HCH	120.0	120.0	120.0
CH_4	r_{CH}	1.092	1.081	1.091
(C_{3v})	∠HCH	109.5	109.5	109.5
CH_2F	r_{CF}	1.33	1.325	
(C_s)	r_{CH}	1.084	1.072	
	∠HCF	114.8	115.0	
	τ(HCFH)	152.2	154.0	
CH_3F	r_{CH}	1.094	1.082	1.095
(C_{3v})	r_{CF}	1.37	1.367	1.391
	∠HCH	109.5	109.7	109.5
	∠FCH	109.4	109.4	
CHF_2	r_{CH}	1.091	1.079	
(C_s)	r_{CF}	1.318	1.312	
	∠FCH	114.2	114.4	
	τ(FCHF)	129.7	130.0	
CH_2F_2	r_{CH}	1.093	1.082	1.092
(C_s)	r_{CF}	1.345	1.341	1.358
	∠HCH	111.7	111.9	111.9
	∠FCH	109.3	109.3	108.3
CF_3	r_{CF}	1.309	1.303	1.33
(C_s)	∠FCF	111.3	111.4	112.0
	τ(FCFF)	124.8	125.1	
CHF_3	r_{CH}	1.09	1.09	1.095
(C_{3v})	r_{CF}	1.325	1.325	1.391
	∠HCF	110.5	110.5	109.5

H_2, BHLYP bond distance at cc-pVDZ basis set is predicted to be 0.013 Å longer than the experimental one,[39] while it is 0.004 Å shorter at the cc-pVTZ basis set. For C−H bond, the largest errors are 0.004 and 0.01 Å for the cc-pVDZ and cc-pVTZ basis set, respectively. The C−F bond distances computed at two different basis sets are pretty close and are lower than the available experimental data by about 0.02 Å. The computed bond angles are seen to be practically same at two different basis sets and are very close to the experimental available data. On the basis of these results, we have chosen the cc-pVDZ basis set for calculations of structure and Hessian information along the MEP for rate calculations later.

Table 2 lists geometrical parameters of the transition state structures for the four H abstraction reactions calculated with the BHLYP method using two different basis sets. Similar to the H + CH_4 reaction, the H + HCF_3 reaction also has a C_{3v} transition state. The other two reactions, H + CH_2F_2 and H + CH_3F, have C_s transition states. These transition states were confirmed with normal-mode analysis to have only one imaginary frequency whose eigenvector corresponds to the direction of the reaction. The computed geometrical parameters for the transition states for all four reactions at both cc-pVDZ and cc-pVTZ basis sets yield small differences. The maximum difference in the H′−H″ bond distance is 0.005 Å in $FH_2C\cdots H'\cdots H''$. The maximum difference in the C−H′ bond is 0.026 Å in $F_3C\cdots H'\cdots H''$. The difference in computed bond angle for ∠H′H″C at two different basis sets is seen to be within 0.8°. One can easily notice that the active coordinates in these reactions, namely, the C−H′ bond distance ($r_{CH'}$) and H′−H″ distance ($r_{H'H''}$) are similar for reactions that the same symmetry. Our present results are consistent with previous MP2/6-31G(d) data from Berry et al.[5] Table 3 lists BHLYP/cc-pVDZ frequencies and available experimental data at stationary states. For H_2, the computed frequency is about 2% larger than the experimental value. For the rest of the systems the computed frequencies are 4−6% larger than the experimental data.[39]

TABLE 2: A Comparison of the Calculated Geometrical Parameters (Distances in angstroms and Angles in degrees) of the Transition States for the Selected Hydrogen Abstraction Reactions[a]

level/basis set	geometrical parameters	$H_3C\cdots H'\cdots H''$ (C_{3v})	$FH_2C\cdots H'\cdots H''$ (C_s)	$F_2HC\cdots H'\cdots H''$ (C_s)	$F_3C\cdots H'\cdots H''$ (C_{3v})
BHLYP/cc-pVDZ	$r_{H'H''}$	0.896 (0.878)	0.931	0.932 (0.901)	0.897 (0.879)
	$r_{CH'}$	1.415 (1.424)	1.369	1.365 (1.395)	1.412 (1.423)
	r_{CH}	1.087	1.091	1.093	
	r_{CF}		1.344	1.327	1.312
	∠H′H″C	180.0	177.3	176.1	180.0
	∠HCH′	103.1	104.4	108.7	
	∠FCH′		107.4	106.9	108.7
BHLYP/cc-pVTZ	$r_{H'H''}$	0.897	0.926	0.928	0.895
	$r_{CH'}$	1.384	1.349	1.345	1.386
	r_{CH}	1.076	1.079	1.082	
	r_{CF}		1.341	1.322	1.309
	∠H′H″C	180.0	176.5	175.4	180.0
	∠HCH′	103.4	104.9	106.8	
	∠FCH′		118.9	109.2	108.7

[a] Values in parentheses are MP2/6-31G(d) data taken from ref 5.

TABLE 3: Calculated and Experimental Frequencies (cm^{-1}) at the Stationary Points

	BHLYP/cc-pVDZ	exptl
H_2	4480	4401
CH_3	3386,3190,1424,457	3184,3002,1383,580
CH_4	3238,3112,1583,1361	3018,2917,1534,1306
$H_3C\cdots H\cdots H$ (TS)	3318,3156,1933,1450, 1127,1082,540, 1307i	
CH_2F	3380,3219,1505,1329, 1202,612	
CH_3F	3210,3121,1531,1520, 1226,1133	3006,2965,1467, 1464,1182,1049
$FH_2C\cdots H\cdots H$ (TS)	3278,3161,1697,1512, 1258,1241,1190,1110, 532,297,1494i	
CHF_2	3223,1400,1252,1232, 1031,570	
CH_2F_2	3220,3151,1572,1523, 1320,1212,1191,1178, 546	3013,2949,1508, 1435,1262,1176, 1116,1090
$F_2HC\cdots H\cdots H$ (TS)	3194,1688,1426,1276, 1241,1200,1185,1099, 566,352, 279,1533i	
CF_3	1351,1143,723,528	1259,1090,701,500
CHF_3	3244,1456,1244,1193, 726, 528	3035,1376,1152, 1137,700, 508
$F_3C\cdots H\cdots H$ (TS)	1897,1343,1131,1073,705, 531,267,1417i	

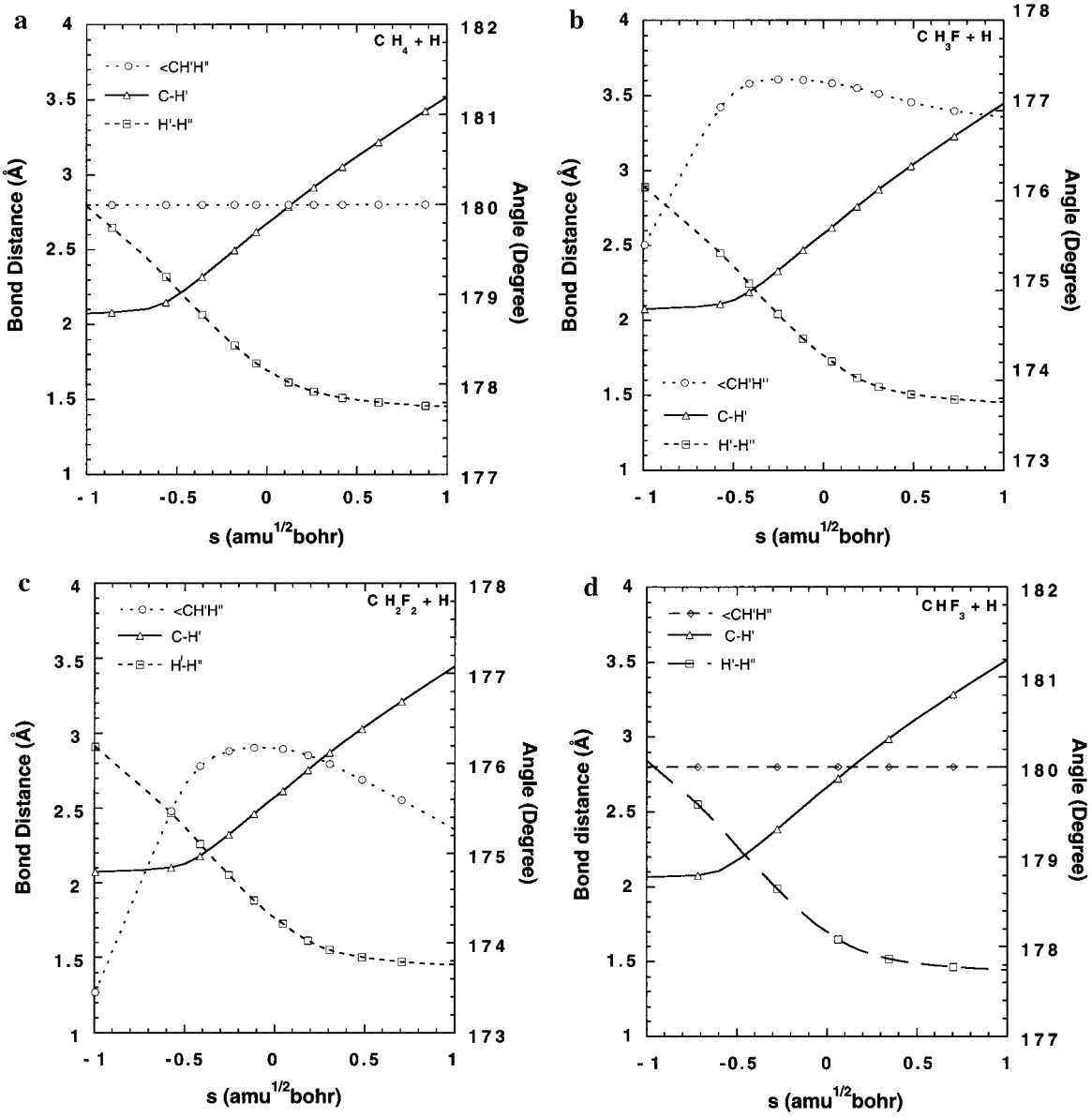

Figure 1. (a) Selected geometrical profiles along the BHLYP/cc-pVDZ minimum energy path for the $CH_4 + H \leftrightarrow CH_3 + H_2$ reaction plotted vs the reaction coordinate s in the mass weighted coordinates. (b) Same types of geometrical profiles as those in a for the $CH_3F + H \leftrightarrow CH_2F + H_2$ reaction. (c) Same types of geometrical profiles as those in a for the $CH_2F_2 + H \leftrightarrow CHF_2 + H_2$ reaction. (d) Same types of geometrical profiles as those in a for the $CHF_3 + H \leftrightarrow CF_3 + H_2$ reaction.

The reaction energies and barrier heights for all the four H abstraction reactions computed at MP4 and PMP4 levels are listed in Table 4. Differences in the energies computed at MP4 and PMP4 level indicate the effects of the spin contamination. The largest error due to spin contamination in the reaction energies is about 0.7 kcal/mol for the $H + CH_4$ reaction. Spin contamination is more severe in the transition state regions. As a result, the differences in the MP4 and PMP4 results for the barrier heights are much larger. Consequently, PMP4 barriers are generally about 2 kcal/mol lower than the MP4 values. Zero-point energy corrections were found to lower these barriers by the order of 2 kcal/mol in these reactions. It is interesting to point out that reactions with the same symmetry not only have similar transition state structures but also similar barrier heights. And the higher symmetry reactions, i.e., $H + CH_4$ and $H + HCF_3$, have larger barriers by about 2 kcal/mol. No trend with respect to the number of F substituent is observed. Similar observations were also reported by Berry et al.[5] Though the barriers calculated by Berry et al. are about 2 kcal/mol too large compared to our results, these differences could result from combinations of differences in geometry, in the treatment of electron correlation and spin contamination between G2 and our procedure, PMP4/cc-pVTZ//BHLYP/cc-pVDZ. Finally, the

TABLE 4: Calculated PMP4 Reaction Energies ΔE, Reaction Enthalpies at 298 K $\Delta H°$, Classical Barrier Heights $\Delta V^{\ddagger}$, and Zero-Point Energy Corrected Barrier Heights $\Delta V_a^{G,\ddagger}$ (kcal/mol) for the Selected Hydrogen Abstraction Reactions

	$CH_4+H \rightarrow CH_3+H_2$	$CH_3F+H \rightarrow CH_2F+H_2$	$CH_2F_2+H \rightarrow CHF_2+H_2$	$CHF_3+H \rightarrow CF_3+H_2$
ΔE	3.10 (3.83)[a]	−0.87 (−0.18)	−0.48 (−0.05)	4.61 (4.94)
$\Delta H°$	1.99	−1.66	−0.88	4.51
exptl	0.55[b]	-3.7 ± 2	-1.10 ± 0.9	0.1
$\Delta V^{\ddagger}$	14.58 (16.48)	12.61 (14.59)	12.58 (14.57)	15.50 (17.50)
$\Delta V_a^{G,\ddagger}$	12.90	10.72	10.45	13.31
	14.64[c]	12.87	12.58	15.12

[a] Values in parentheses are from MP4 calculations. [b] Experimental values derived from heats of formation taken from CRC Handbook of *Physics and Chemistry*, 79th ed.; CRC Press: Boca Raton, FL, 1998. [c] Values in this row are taken from ref 5.

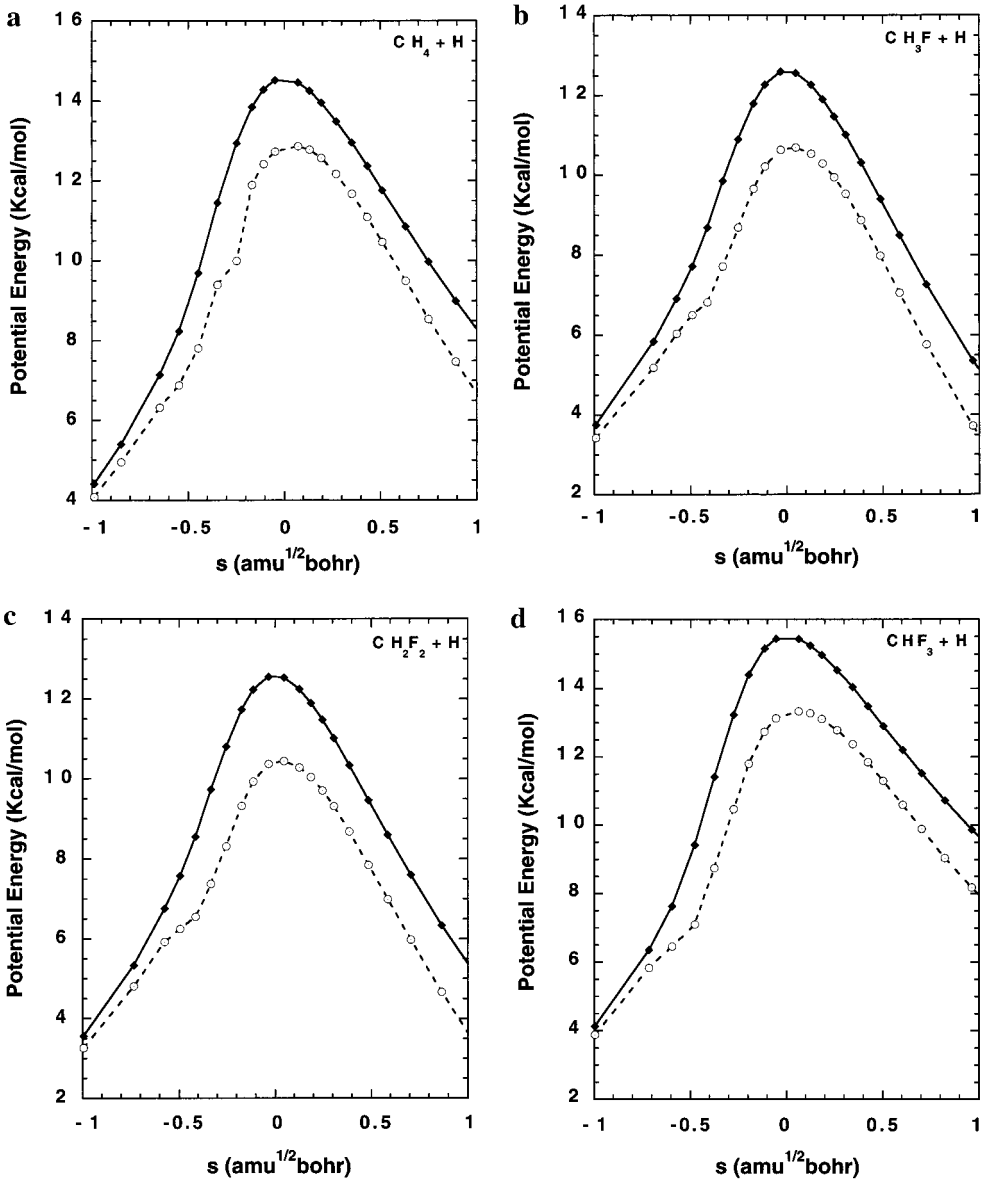

Figure 2. (a) The classical potential energy $V_{MEP}(s)$ (solid line) and the vibrationally ground-state adiabatic potential energy $V_a^G(s)$ (dashed line) curves along the BHLYP/cc-pVDZ minimum energy path for the $CH_4 + H \leftrightarrow CH_3 + H_2$ reaction plotted vs the reaction coordinate *s*. (b) Same types of curves as those in a for the $CH_3F + H \leftrightarrow CH_2F + H_2$ reaction. (c) Same types of curves as those in a for the $CH_2F_2 + H \leftrightarrow CHF_2 + H_2$ reaction. (d) Same types of curves as those in a for the $CHF_3 + H \leftrightarrow CF_3 + H_2$ reaction.

calculated reaction enthalpies at 298 K are in reasonable agreement with the experimental data derived from the heats of formation except for the reaction enthalpy derived from the $H + CHF_3$ reaction where we predicted it to be 4.51 kcal/mol endothermic while experimentally it is nearly thermal neutral. Consequently, we anticipated that our calculated rate constants for the reverse $H_2 + CF_3$ reaction would be too large.

II. Minimum Energy Path. Figures 1 and 2 display how certain properties vary as functions of the reaction coordinate. Figure 1a−d show the structural changes of the active C−H′ and H′−H″ bonds and the ∠CH′H″ angle along the reaction coordinate *s*. In all the four reactions, it is seen that the C−H′ bond distance remains insensitive up to certain stage of the MEP ($s = -0.6$ amu$^{1/2}$ bohr) and then increases smoothly up to ∼3.5 Å along MEP from its value of ∼2.1 Å. However, the H′−H″ bond distance decreases smoothly to a H−H bond distance of 1.45 Å. The ∠CH′H″ angle passes through a maxima along the MEP in case of reactions with CH_3F and CH_2F_2, i.e., for the reactions which pass through C_s transition state. For the other two reactions which have C_{3v} transition state symmetry, the ∠CH′H″ angle remains equal to 180.0° along the reaction coordinate to preserve the symmetry. Figures 2a−d depict the classical potential energy (solid line) and vibrationally adiabatic ground state potential energy (dotted line) curve along the MEP for the H atom abstraction reactions with four different species, namely CH_4, CH_3F, CH_2F_2, and CHF_3, respectively.

III. Rate Constants. CVT rate calculations including different tunneling (ZCT and SCT) contributions were carried out for both forward and reverse directions for all four H abstraction reactions in the temperature range of 200−1000 K. Figure 3a−d display the Arrhenius plots of the calculated results along with the available experimental data for the H atom abstraction reactions with CH_4, CH_3F, CH_2F_2, and CHF_3, respectively. Figure 4a−d show the Arrhenius plots for the corresponding reverse reactions. Recrossing effects were found to be rather small compared to the tunneling effects. This is somewhat expected due to rather large barriers of these reactions. Similar to our previous study, excellent agreement is observed between the present CVT/SCT results with the experimental data over a wide range of temperature (see Figure 3a) for the forward

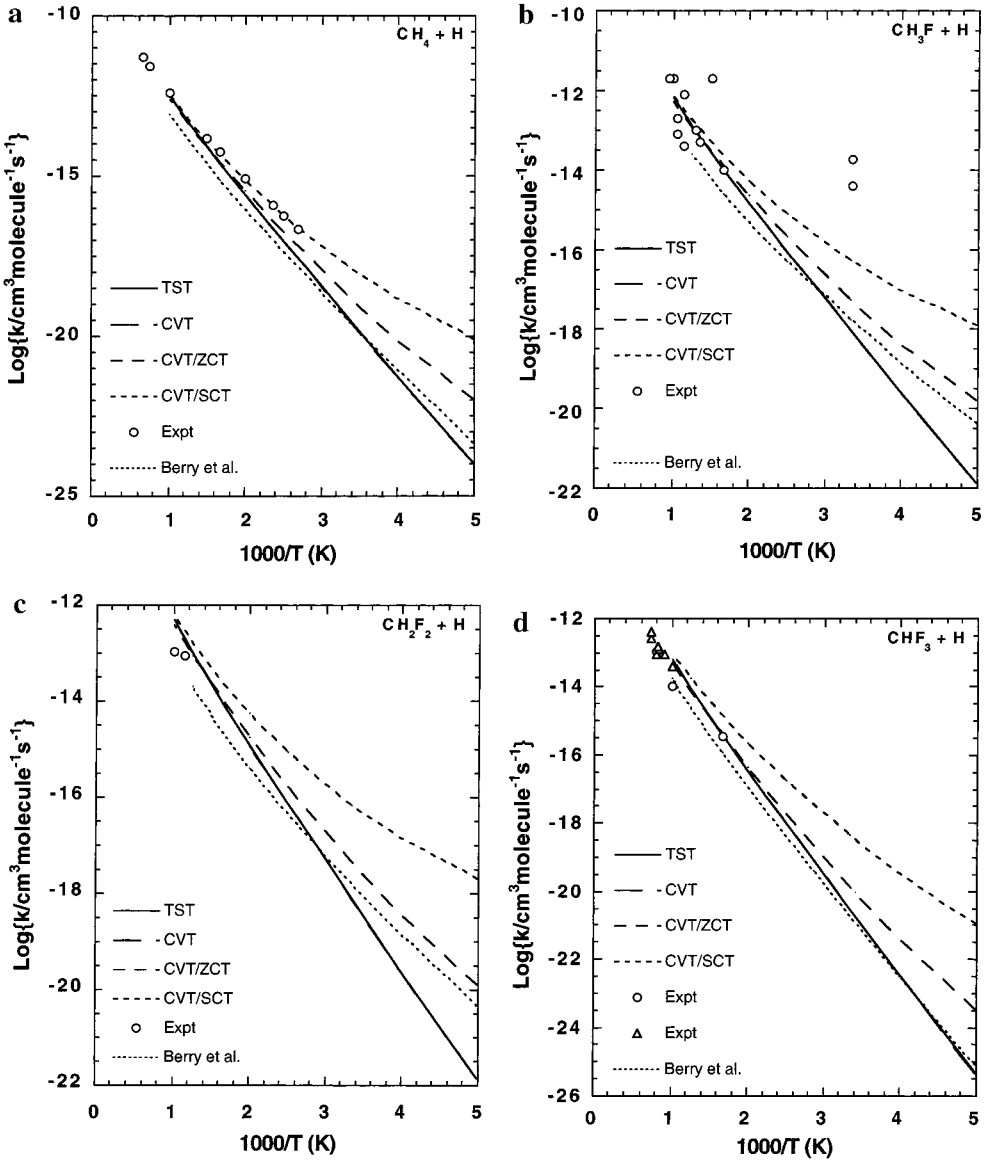

Figure 3. (a) Comparison of Arrhenius plots of the calculated forward rate constants versus 1000/*T* and available experimental data for the $CH_4 + H \leftrightarrow CH_3 + H_2$ reaction. The solid line shows the calculated results from TST, long dashed line from CVT, dashed line from CVT/ZCT, short dashed line from CVT/SCT, dotted line from the calculated results by Berry et al. (ref 5), and the open circles from the experimental results. (b) Same types of plots as those in a for the $CH_3F + H \leftrightarrow CH_2F + H_2$ reaction. (c) Same types of plots as those in a for the $CH_2F_2 + H \leftrightarrow CHF_2 + H_2$ reaction. (d) Same types of plots as those in a for the $CHF_3 + H \leftrightarrow CF_3 + H_2$ reaction. Open triangles show recent experimental data by Hranisavljevic et al. (ref 19).

reaction of $CH_4 + H \rightarrow CH_3 + H_2$. For the $CH_3F + H \rightarrow CH_2F + H_2$ reaction (see Figure 3b), there is a large scattering in experimental data, though our calculated rate constants are in reasonable agreement with the experimental data in the high-temperature range.[6,9] There is only one set of experimental data[6] available for the $CH_2F_2 + H \rightarrow CHF_2 + H_2$ reaction and they are reasonably close (difference in $\Delta\log k \sim 0.6$) to the calculated profile (see Figure 3c). There are several sets of experimental data[6,8,19] available for the $CHF_3 + H \rightarrow CF_3 + H_2$ reaction in the high-temperature range. Our calculate rate constants agree well with these data. The experimental data in the plot shows that the rate constant measured at the same temperature has a deviation of $\Delta\log k \sim 0.5$. The calculated CVT/SCT results do show that there are large tunneling effects in the H-abstraction reactions of fluoromethanes. However, no experimental data are available in the lower temperature range to compare with the computed data for these reactions. Note that the dotted lines in Figure 3a−d are the Arrhenius curves prescribed by Berry and co-workers based on their G2-(ZPE=MP2) calculations with one-dimensional tunneling corrections for the forward H-abstraction reactions.[5] One can see from the Figure 3a that Berry et al.'s results are substantially smaller than the experimental data particularly at low temperatures. This indicates that tunneling effects were not accurately accounted in such calculations. Table 5 lists thermal rate constants calculated at the CVT/SCT level for the four forward reactions. Notice that the rate of the reaction of H atom with CH_4 is much slower than its mono- or difluorine substituted counterpart over the whole temperature range. However, in the case of trifluorine substituted system (CHF_3), the rate constant is predicted to be lower than that even with CH_4, indicating its inertness toward H abstraction.

For the reverse reactions (see Figure 4a−d and Table 6), similar conclusions can be made for comparisons with available experimental data and previous calculations. Note that, for the $CH_2F + H_2$ reaction, there is no experimental data available for comparison. For the $CF_3 + H_2$ reaction, there are several sets of experimental data[11−16,18−19] available and the measured

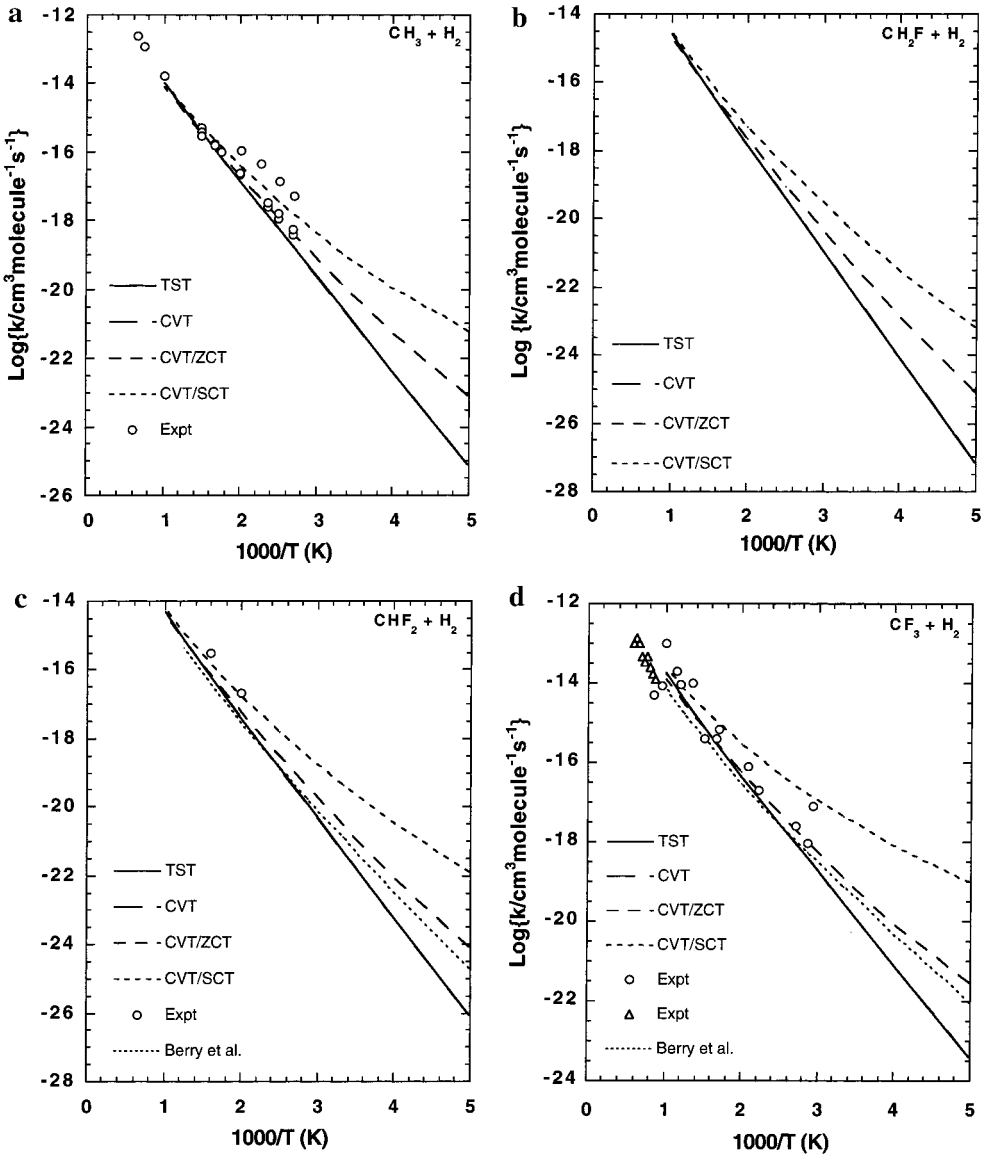

Figure 4. (a) Comparison of Arrhenius plots of the calculated reverse rate constants vs $1/T$ at different methods and available experimental data for the $CH_4 + H \leftrightarrow CH_3 + H_2$ reaction. Descriptions of lines and symbols are the same as in Figure 3a. Same types of plots as those in Figure 3b for the reverese reaction. (c) Same types of plots as those in Figure 3c for the reverse reaction. (d) Same types of plots as those in Figure 3d for the reverse reaction.

TABLE 5: CVT/SCT Forward Rate Constants (k_f) (cm^3 molecule^{-1} s^{-1}) for the Selected Hydrogen Abstraction Reactions

T (K)	$CH_4 + H \rightarrow CH_3 + H_2$	$CH_3F + H \rightarrow CH_2F + H_2$	$CH_2F_2 + H \rightarrow CHF_2 + H_2$	$CHF_3 + H \rightarrow CF_3 + H_2$
200	7.60×10^{-21}	1.17×10^{-18}	1.91×10^{-18}	1.08×10^{-21}
250	1.43×10^{-19}	9.42×10^{-18}	1.37×10^{-17}	3.38×10^{-20}
300	1.55×10^{-18}	5.27×10^{-17}	6.97×10^{-17}	4.53×10^{-19}
350	1.12×10^{-17}	2.26×10^{-16}	2.73×10^{-16}	3.50×10^{-18}
400	5.84×10^{-17}	7.74×10^{-16}	8.71×10^{-16}	1.83×10^{-17}
450	2.32×10^{-16}	2.21×10^{-15}	2.34×10^{-15}	7.19×10^{-17}
500	7.43×10^{-16}	5.46×10^{-15}	5.50×10^{-15}	2.27×10^{-16}
600	4.72×10^{-15}	2.35×10^{-14}	2.21×10^{-14}	1.41×10^{-15}
800	5.85×10^{-14}	1.81×10^{-13}	1.56×10^{-13}	1.71×10^{-14}
1000	3.07×10^{-13}	7.15×10^{-13}	5.86×10^{-13}	8.90×10^{-14}

data has a deviation as large as $\Delta \log k \sim 1.5$ at certain temperature. Our CVT/SCT results appear to be too large. It is somewhat expected because our calculated enthalpy of reaction is rather large compared to experimental data (4.51 versus 0.10 kcal/mol) making the reverse barrier too low for this reaction. However, the large scattering in the experimental data also warrants that more measurements are needed.

TABLE 6: CVT/SCT Reverse Rate Constants (k_r) (cm^3 molecule^{-1} s^{-1}) for the Selected Hydrogen Abstraction Reactions

T (K)	$CH_4 + H \rightarrow CH_3 + H_2$	$CH_3F + H \rightarrow CH_2F + H_2$	$CH_2F_2 + H \rightarrow CHF_2 + H_2$	$CHF_3 + H \rightarrow CF_3 + H_2$
200	5.61×10^{-22}	6.16×10^{-24}	1.20×10^{-22}	9.44×10^{-20}
250	1.08×10^{-20}	3.10×10^{-22}	3.49×10^{-21}	7.81×10^{-19}
300	1.13×10^{-19}	5.66×10^{-21}	4.35×10^{-20}	4.18×10^{-18}
350	7.70×10^{-19}	5.46×10^{-20}	3.17×10^{-19}	1.64×10^{-17}
400	3.72×10^{-18}	3.37×10^{-19}	1.58×10^{-18}	5.10×10^{-17}
450	1.37×10^{-17}	1.49×10^{-18}	5.97×10^{-18}	1.32×10^{-16}
500	4.07×10^{-17}	5.18×10^{-18}	1.82×10^{-17}	2.98×10^{-16}
600	2.26×10^{-16}	3.64×10^{-17}	1.07×10^{-16}	1.11×10^{-15}
800	2.26×10^{-15}	5.01×10^{-16}	1.20×10^{-15}	6.98×10^{-15}
1000	1.03×10^{-14}	2.78×10^{-15}	5.99×10^{-15}	2.49×10^{-14}

Conclusions

We have presented the results of direct ab initio dynamics calculations of thermal rate constants of H-abstraction reactions of hydrogen atom with fluoromethanes (CH_3F, CH_2F_2, and CHF_3). Effects of fluorine substitution on the reaction rate have been examined. Dynamical calculations are based on a full

variational transition state theory plus multidimensional semiclassical tunneling corrections with the potential energy information calculated directly from a combination of PMP4 and BHLYP DFT methods. We found that the activation energies for these reactions do not correlate with the number of fluorine substitution but rather with the symmetry of the reaction. Reactions with the same symmetry have similar transition state structure and barrier height.

The calculated rate constants of these reactions are in good agreement with the available experimental data for both forward and reverse directions for a wide range of temperatures. We have found that tunneling effects are significant for all the reactions studied.

Acknowledgment. This work is supported in part by the National Science Foundation (Grant CHE-9527333) and by the University of Utah Center for the Simulation of Accidental Fires & Explosions, funded by the Department of Energy, Lawrence Livermore National Laboratory, under Subcontract B341493. An allocation of computer time from the Center for High Performance Computing is gratefully acknowledged.

References and Notes

(1) Ravishankara, A. R.; Turnipseed, A. A.; Jensen, N. R.; Barone, S.; Mills, M.; Howard, C. J.; Solomon, S. *Science* **1994**, *263*, 71.

(2) Ko, M. K. W.; Sze, N.-D.; Rodriguez, J. M.; Weistenstein, D. K.; Heisey, C. W.; Wayne, R. P.; P., B.; Canosa-Mas, C. E.; Sidebottom, H. W.; Treacy, J. *Geophys. Res. Lett.* **1994**, *21*, 101.

(3) Fallon, G. S.; Chelliah, H. K.; Linteris, G. T. In *Proceedings of the 25th International Symposium on Combustion*; The Combustion Institute: Pittsburgh, 1996; p 1395.

(4) Westmoreland, P. R.; Donald, J.; Burgess, D. R. F.; Zachariah, M. R.; Tsang, W. In *Proceedings of the 25th International Symposium on Combustion*; The Combustion Institute: 1994; p 1505.

(5) Berry, R. J.; Ehlers, C. J.; Burgess, D. R., Jr.; Zachariah, M. R.; Marshall, P. *Chem. Phys. Lett.* **1997**, *269*, 107.

(6) Baulch, D. L.; Duxbury, J.; Grant, S. J.; Montague, D. C. *J. Phys. Chem. Ref. Data 10, Suppl. 1* **1981**, *4*.

(7) Baulch, D. L.; Cobos, C. J.; Cox, R. A.; Esser, C.; Frank, P.; Just, T.; Kerr, J. A.; Pilling, M. J.; Troe, J.; Walker, R. W.; Warnatz, J. *J. Phys. Chem. Ref. Data* **1992**, *21*, 441.

(8) Richter, H.; Vandooren, J.; Tiggelen, P. J. v. In *Proceedings of the 25th International Symposium on Combustion*; The Combustion Institute: Pittsburgh, 1994; p 825.

(9) Jones, W. E.; Ma, J. L. *Can. J. Chem.* **1986**, *64*, 2192.

(10) Pritchard, G. O.; Perona, M. J. *Int. J. Chem. Kinet.* **1969**, *1*, 509.

(11) Ayscough, P. B.; Polanyi, J. C. *Trans. Faraday Soc.* **1956**, *52*, 960.

(12) Fagarash, M. B.; Moin, F. B.; Ocheret'ko, V. I. *Kinet. Katal.* **1968**, *9*, 92.

(13) Berces, T.; Marta, F.; Szilagyi, I. *J. Chem. Soc., Faraday Trans. 1* **1972**, *68*, 867.

(14) Arthur, N. L.; Donchi, K. F.; McDonell, J. A. *J. Chem. Soc. I* **1975**, *71*, 2431.

(15) Kibby, C. L.; Weston Jr., R. E. *J. Chem. Phys.* **1968**, *49*, 4825.

(16) Pritchard, G. O.; Pritchard, H. O.; Schiff, H. I.; Trotman-Dichenson, A. F. *Trans. Faraday Soc.* **1956**, *52*, 848.

(17) Arthur, N. L.; Bell, T. N. *Rev. Chem. Intermed.* **1978**, *2*, 37.

(18) Hidaka, Y.; Nakamura, T.; Kawano, H.; Koike, T. *Int. J. Chem. Kinet.* **1993**, *25*, 983.

(19) Hranisavljevic, J.; Michael, J. V. *J. Phys. Chem. A* **1998**, *102*, 7668.

(20) Fu, Y.; Lewis-Bevan, W.; Tyrrel, J. *J. Phys. Chem.* **1995**, *99*, 630.

(21) Berry, R. J.; Burgess, D. R. F., Jr.; Nyden, M. R.; Zachariah, M. R.; Schwartz, M. *J. Phys. Chem.* **1995**, *99*, 17145.

(22) Schneider, W. F.; Wallington, T. J. *J. Phys. Chem.* **1993**, *97*, 12783.

(23) Truhlar, D. G. In *The Reaction Path in Chemistry: Current Approaches and Perspectives*; Heidrich, D., Ed.; Kluwer Academic: The Netherlands, 1995; p 229.

(24) Truong, T. N.; Duncan, W. T. *J. Phys. Chem.* **1994**, *101*, 7408.

(25) Duncan, W. T.; Bell, R. L.; Truong, T. N. *J. Comput. Chem.* **1998**, *19*, 1039.

(26) Duncan, W. T.; Truong, T. N. *J. Chem. Phys.* **1995**, *103*, 9642.

(27) Bell, R. L.; Truong, T. N. *J. Chem. Phys.* **1994**, *101*, 10442.

(28) Truong, T. N. *J. Chem. Phys.* **1995**, *102*, 5335.

(29) Truong, T. N.; Evans, T. J. *J. Phys. Chem.* **1994**, *98*, 9558.

(30) Truong, T. N.; Duncan, W. T.; Bell, R. L. In *Chemical Applications of Density-Functional Theory*; Americal Chemical Society: Washington, DC, 1996; p 85.

(31) Truhlar, D. G.; Garrett, B. C. *Annu. Rev. Phys. Chem.* **1984**, *35*, 159.

(32) Truhlar, D. G.; Garrett, B. C.; Klippenstein, S. J. *J. Phys. Chem.* **1996**, *100*, 12771.

(33) Truong, T. N.; Truhlar, D. G. *J. Chem. Phys.* **1990**, *93*, 1761.

(34) Lu, D.-h.; Truong, T. N.; Melissas, V. S.; Lynch, G. C.; Liu, Y. P.; Garrett, B. C.; Steckler, R.; Isaacson, A. D.; Rai, S. N.; Hancock, G. C.; Lauderdale, J. G.; Joseph, T.; Truhlar, D. G. *Comput. Phys. Commun.* **1992**, *71*, 235.

(35) Liu, Y.-P.; Lynch, G. C.; Truong, T. N.; Lu, D.-h.; Truhlar, D. G. *J. Am. Chem. Soc.* **1993**, *115*, 2408.

(36) Truong, T. N. *J. Chem. Phys.* **1994**, *100*, 8014.

(37) Frisch, M. J.; Trucks, G. W.; Schlegel, H. B.; Gill, P. M. W.; Johnson, B. G.; Robb, M. A.; Cheeseman, J. R.; Keith, G. A.; A., P. J.; Mongomery, J. A.; Raghavachari, K.; Al-Laham, M. A.; Zakrzewski, V. G.; Ortiz, J. V.; Foresman, J. B.; Cioslowski, J.; Stefanov, B. B.; Nanayakkara, A.; Challacombe, M.; Peng, C. Y.; Ayala, P. Y.; Chen, W.; Wong, M. W.; Andres, J. L.; Replogle, E. S.; Gomperts, R.; Martin, R. L.; Fox, D. J.; Binkley, J. S.; Defrees, D. J.; Baker, J.; Stewart, J. P.; Head-Gordon, M.; Gonzalez, C.; Pople, J. A. *Gaussian 94, Revision B*; Gaussian, Inc.: Pittsburgh, 1995.

(38) Gonzalez, C.; Schlegel, H. B. *J. Phys. Chem.* **1990**, *94*, 5523.

(39) *JANAF Thermochemical Tables*, 2nd ed.; National Standard Reference Data Series; National Bureau of Standards: Washington, DC, 1986; Vol. 37.